Human Molecular Genetics, 2011, Vol. 20, No. 5 **988–999**
doi:10.1093/hmg/ddq544
Advance Access published on December 15, 2010

A novel *Akt3* mutation associated with enhanced kinase activity and seizure susceptibility in mice

Satoko Tokuda[1], Connie L. Mahaffey[1], Bobby Monks[2], Christian R. Faulkner[3], Morris J. Birnbaum[2], Steve C. Danzer[3] and Wayne N. Frankel[1,*]

[1]The Jackson Laboratory, Bar Harbor, ME 04609, USA, [2]Institute for Diabetes, Obesity and Metabolism, University of Pennsylvania School of Medicine, Philadelphia, PA 19104, USA and [3]Department of Anesthesia, Cincinnati Children's Hospital Medical Center, Cincinnati, OH 45229, USA

Received July 23, 2010; Revised November 22, 2010; Accepted December 9, 2010

In a phenotype-driven mutagenesis screen, a novel, dominant mouse mutation, *Nmf350*, caused low seizure threshold, sporadic tonic–clonic seizures, brain enlargement and ectopic neurons in the dentate hilus and molecular layer of the hippocampus. Genetic mapping implicated *Akt3*, one of four candidates within the critical interval. Sequencing analysis revealed that mutants have a missense mutation in *Akt3* (encoding one of three AKT/protein kinase B molecules), leading to a non-synonymous amino acid substitution in the highly conserved protein kinase domain. Previous knockout studies showed that *Akt3* is pivotal in postnatal brain development, including a smaller brain, although seizures were not observed. In contrast to $Akt3^{Nmf350}$, we find that *Akt3* null mice exhibit an elevated seizure threshold. An *in vitro* kinase assay revealed that $Akt3^{Nmf350}$ confers higher enzymatic activity, suggesting that $Akt3^{Nmf350}$ might enhance AKT signaling in the brain. In the dentate gyrus of $Akt3^{Nmf350}$ homozygotes, we also observed a modest increase in immunoreactivity of phosphorylated ribosomal protein S6, an AKT pathway downstream target. Together these findings suggest that $Akt3^{Nmf350}$ confers an increase of AKT3 activity in specific neuronal populations in the brain, and a unique dominant phenotype. $Akt3^{Nmf350}$ mice provide a new tool for studying physiological roles of AKT signaling in the brain, and potentially novel mechanisms for epilepsy.

INTRODUCTION

Epilepsy, defined by recurrent seizures resulting from abnormal, synchronized neuronal discharges in the brain, affects up to 1% among the population. A genetic contribution to the disease has been estimated for about 40% of epilepsy patients (1). In recent years, advanced genetic approaches, such as association studies of candidate genes and genome-wide linkage studies with patients or family cases, have provided a better understanding of the genetic basis of idiopathic generalized epilepsies, with the identification of more than 20 variants involved in these disorders (2). The majority of responsible genes, however, remain unidentified because of the multifactorial etiology and genetic heterogeneity of the disease.

Phenotype-based chemical mutagenesis with ethylnitrosourea (ENU) has been performed with high success and efficiency to obtain new animal models of various neurological disorders and to discover human disease genes (3–7). The electroconvulsive threshold (ECT) test in mice has been used extensively to advance the study of human seizures, and is an integral part of the ongoing program for development of antiepileptic drugs. We adopted ECT as a robust screening tool to find seizure-prone or resistant genes following ENU mutagenesis. Using this approach, we previously discovered that a dominant mutation, *Szt1*, lowers the seizure threshold in mice without spontaneous seizures (8). Interestingly, genetic analysis revealed that the *Szt1* mutation was a spontaneous deletion that included the *Kcnq2* gene, the human orthologue of which is mutated in human epilepsy families. This provided proof of principle that ECT can be a relevant screening tool to develop genetic models that are relevant for human epilepsy research.

Upstream and downstream molecules involved in serine/threonine kinase AKT pathways have been implicated in mechanisms of epilepsy (9–13). AKT, also known as

*To whom correspondence should be addressed at: The Jackson Laboratory, 600 Main Street, Bar Harbor, ME 04609-1500, USA. Tel: +1 2072886354; Fax: +1 2072886780; Email: wayne.frankel@jax.org

protein kinase B (PKB), is a critical signaling molecule in the phosphatidylinositol 3 kinase (PI3K) pathway involved in diverse cellular process such as cell survival, growth, proliferation, metabolism and migration (14,15). Recent reports have emphasized the new roles for AKT in neurobiology, such as in brain development, synaptic plasticity and neurodegeneration (16–20). Upregulation of AKT has been also implicated in neuroprotection and neurogenesis after brain injuries such as stroke and seizures in both rodents and humans (21–24). Of the three AKT genes expressed in mammalian cells: AKT1 (PKBα), AKT2 (PKBβ) and AKT3 (PKBγ), AKT3 is the most prominent in the brain and testis, while AKT1 is ubiquitous, and AKT2 predominantly expressed in the liver, skeletal muscle and adipose tissues. Targeted disruption of each isoform in mice has been reported. *Akt1* null mice display placental hypotrophy and a reduction in body weight, while *Akt2* deficient mice exhibit a diabetes-like syndrome with mild growth retardation (19,25–27). *Akt3* null mice show a selective reduction in brain size—25% smaller than wild-type brains with no difference in body size—suggesting that *Akt3* plays a crucial role in postnatal brain development (16,17). Previously, *Akt3* gene mutations have been reported in melanoma tumor cell lines but not in neurological diseases such as epilepsy (28). On the other hand, altered mammalian target of rapamycin (mTOR) signaling, one of the major downstream pathways of AKT, is observed not only in a mouse model of tuberous sclerosis complex (TSC, characterized by dysplastic and enlarged neurons, reduced myelination, seizure activity and limited survival), but also in experimental epilepsy models, such as kainate-induced status epilepticus in rats (9–11). Similarly, conditional knockout mice for *Pten*, which is a negative regulator of AKT, have seizures and increased brain size (12,13,29). Notably, an increase in the phosphorylation level of AKT, and of one particular downstream molecule, ribosomal protein S6, has been observed in these models corresponding to activated mTOR signaling. In addition, their seizures were commonly suppressed by the mTOR inhibitor, rapamycin, suggesting that AKT/mTOR pathways mediate mechanisms underlying epileptic seizures. However, isoform-specific roles of AKT in the brain have not been fully clarified (10,30).

Here, we report a missense mutation in the *Akt3* gene, originally detected as showing a low threshold to ECT inherited in a dominant fashion. To determine the role of $Akt3^{Nmf350}$, we further characterized the seizure threshold and brain anatomy of $Akt3^{Nmf350}$ mutant mice compared with *Akt3* null mice. We also assessed kinase activity of mutant AKT3 expressed in human embryonic kidney (HEK) culture cells and investigated increased phosphorylation activities involved in the AKT pathway *in vivo* by western blotting and phospho-S6 immunofluorescence.

RESULTS

A novel ENU-induced missense mutation in Akt3

The *Nmf350* mutation was found to reduce the ECT in a neurological phenotype screen of ENU-mutagenized progeny. Nmf350 mice displayed generalized, tonic–clonic seizures or maximal tonic hindlimb extension seizures in response to transcorneal electrical stimulation at a stimulus setting where approximately 3% of the wild-type C57BL/6J (B6) population reach a generalized tonic–clonic seizure (female, 6.5 mA; male, 8.0 mA) (31). In an initial secondary screen, two of the four mice from a mutant family but none of the seven control B6 mice exhibited generalized, tonic–clonic seizures after treatment with the non-competitive $GABA_A$ antagonist, pentylenetetrazol (PTZ). Spontaneous seizures were also observed sporadically during cage changing in mutant mice older than 6 months of age, but no interictal epileptic EEG were observed in overnight EEG recording (data not shown). The epileptic behaviors in these mice were similar to those commonly described in other mouse strains with handling-associated seizures (32–34), and began with a limbic phase (jaw clonus, ventral then dorsal neck flexion, forelimb paddling/clonus), followed by a generalized phase including the loss of posture, Straub tail and excessive salivation and ending in a prolonged quiescent period. In preliminary studies, no anatomical defects were detected using conventional histology except for the absence of the corpus callosum in two mutant animals. These preliminary data were collected prior to 2006 as part of the former Jackson Laboratory Neuroscience Mutagenesis Facility (NMF; http://www.jax.org/nmf).

In order to map the *Nmf350* mutation, B6J-*Nmf350*/+ heterozygotes were mated to BALB/cByJ (BALB) mice, which have a similar seizure threshold as B6J (31), and affected F_1 hybrids were backcrossed to normal BALB mice. Forty-four backcross or N_2 progeny were used for a whole genome scan using SNP markers, resulting in a potential association on distal Chromosome 1 (data not shown). To confirm the association and to narrow the critical interval, additional informative recombinant mice and their N_3 progeny were ECT-tested. A very strong association (peak LOD score = 14.929) was detected between *D1Frk9* and *D1Mit115* (at 178.5 and 179.5 Mb, respectively; Fig. 1A). These efforts resulted in a 1 Mb critical interval that contained four candidate genes; *Cep170* (centrosomal protein 170), *Sdccag8* (serologically defined colon cancer antigen 8), *Akt3* (thymoma viral proto-oncogene 3) and *Zfp238* (zinc finger protein 238; Fig. 1B). Because a neurological abnormality had been reported in *Akt3* knockout mice (16,17), and because of its very strong expression in the adult hippocampus and cerebral cortex in particular, *Akt3* was considered the best candidate for *Nmf350*. Sequencing of all *Akt3* exons identified a single A to T substitution in codon 219, which predicts an amino acid substitution of aspartic acid to valine (D219V; Figs 1C and 2A). D219 is located in the kinase domain of PKBγ/AKT3 and is evolutionally conserved among different species and other kinase family members at corresponding positions (Fig. 2A and B). AKT3 protein levels in whole brain extracts from both *Nmf350* heterozygous and homozygous mice were not different from wild-type mice (Fig. 2C). No candidate mutations were identified in a complete survey of the coding exons of the remaining three candidate genes (data not shown).

$Akt3^{Nmf350}$ and $Akt3^{tm1Mbb}$ (null) mutants have opposite seizure thresholds

The seizure threshold characteristics observed initially by NMF personnel were then examined in more detail.

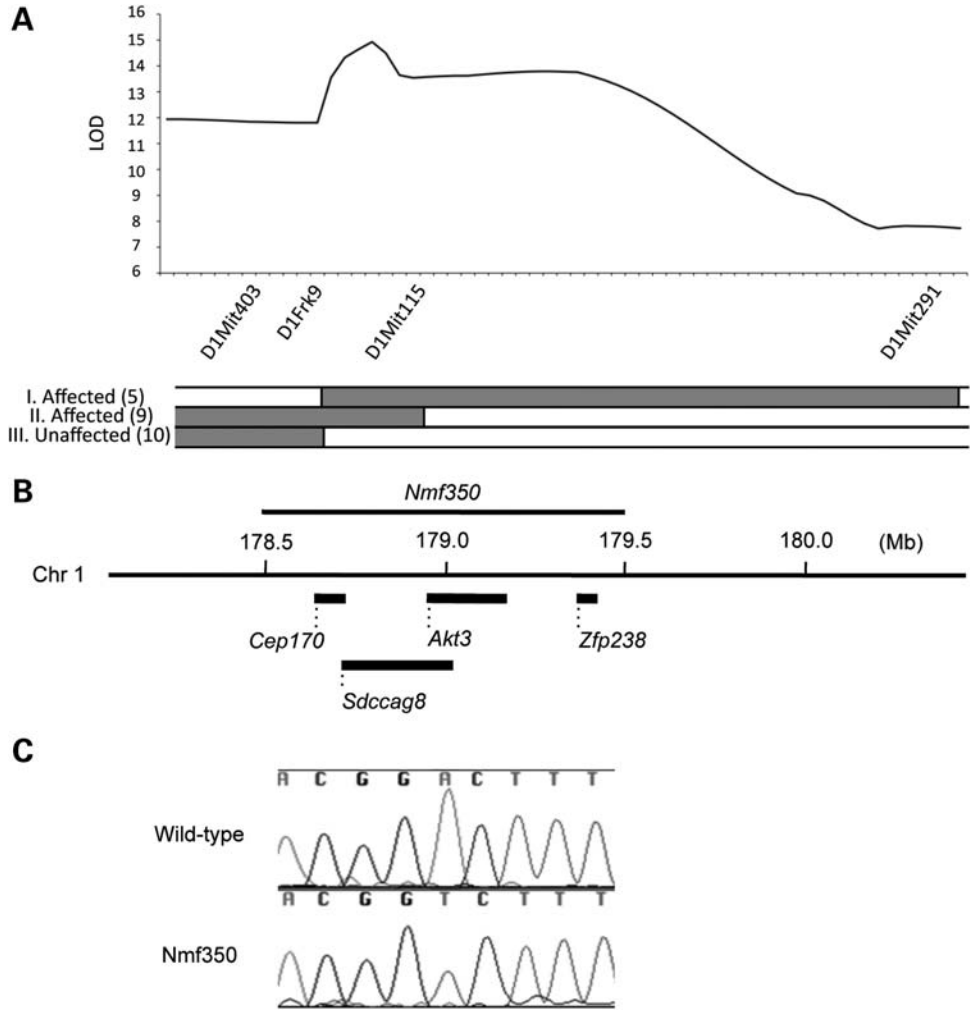

Figure 1. A single nucleotide substitution in *Akt3*. (**A**) Map position of *Nmf350* on chromosome (Chr) 1. N_2 ($n = 58$) mice were genotyped with the indicated SSLP markers and phenotyped by ECT tests. The highest linkage was obtained between *D1Frk9* and *D1Mit115* with a peak LOD score of 14.929, and the critical interval was refined further by progeny testing. The panel below the LOD graph shows genotypes of informative N_2 recombinants (I–III) between *D1Frk9* and *D1Mit115*, which were used for progeny testing: gray, B6J and BALB heterozygous; white, BALB homozygous. The number in parenthesis indicates the number of N_3 progeny inheriting the same genotype and showing the same phenotype as their N_2 parents. (**B**) Physical map of the *Nmf350* locus. The *Nmf350* locus corresponded to a 1 Mb segment on the distal Chr 1, containing four candidate genes. (**C**) The A to T substitution found in exon 8 in the *Akt3* gene by genomic sequencing.

The mean threshold to generalized tonic–clonic seizures was determined in $Akt3^{Nmf350}$ heterozygotes, $Akt3^{Nmf350}$ homozygotes and wild-type littermate or normal B6J mice at 6 weeks of age. As expected, in both males and females, the mean threshold for generalized, tonic–clonic seizures was significantly lower in $Akt3^{Nmf350}$ heterozygous and homozygous mice than in wild-type animals ($P < 0.01$). The seizure thresholds in mA ($\pm$SEM) for females were 6.3 ± 0.2 ($n = 5$), 6.0 ± 0.3 ($n = 8$) and 7.5 ± 0.3 ($n = 5$) mA in $Akt3^{Nmf350/+}$, $Akt3^{Nmf350/nmf350}$ and $Akt3^{+/+}$, respectively; for males, 7.1 ± 0.3 ($n = 4$), 6.8 ± 0.4 ($n = 6$) and 8.8 ± 0.3 ($n = 3$) mA in $Akt3^{Nmf350/+}$, $Akt3^{Nmf350/nmf350}$, and $Akt3^{+/+}$, respectively (Fig. 3). During the establishment of the Nmf350 colony and ECT testing at these thresholds, several mice were noted to progress rapidly past the minimal seizure response to maximal tonic hindlimb extension. In the test group alone, we also observed the same phenomenon in three mutant mice but in none of the wild-type mice. Because maximal seizure responses were induced at stimulus settings that correspond to the 0.02% (female) or 0.0002% (male) response level in wild-type B6J, these observations further underscore the mutant's susceptibility. We also confirmed that $Akt3^{Nmf350}$ heterozygotes and homozygotes have a lower threshold to PTZ-induced seizures; following PTZ injection at a low dose of 40 mg/kg, three of the five $Akt3^{Nmf350}$ heterozygotes and five of the six homozygotes exhibited generalized tonic–clonic seizures (with tonic hindlimb extension observed in one heterozygote and three homozygotes) compared with none of the seven wild-type animals showing any generalized seizure ($P < 0.0003$, Fisher's exact test, Table 1).

Given the identity of the Nmf350 mutation in *Akt3*, it seemed noteworthy that spontaneous seizures were not reported in prior studies of *Akt3* null mutants (16,17), nor did we ever observe seizures in our *Akt3* null colony. Nevertheless, seizure susceptibility had not been proactively assessed in *Akt3* null mutants.

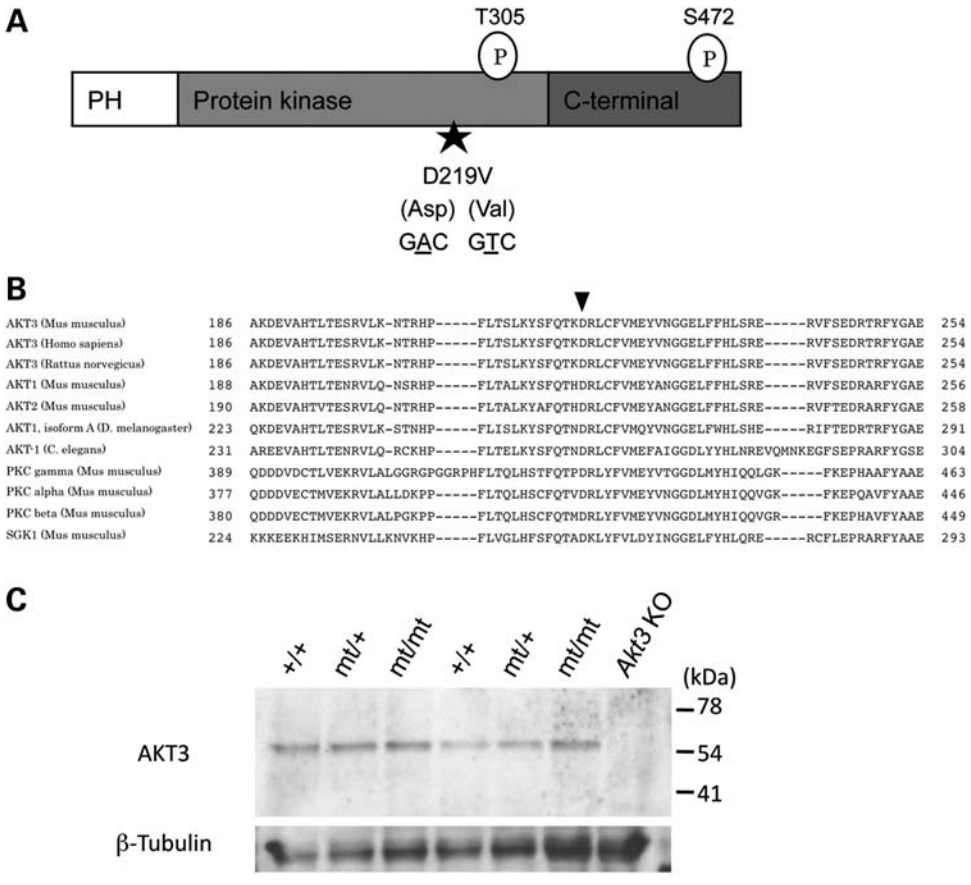

Figure 2. The missense mutation found in Nmf350 mice is located in the protein kinase domain of AKT3. (**A**) Schematic figure of the protein structure of AKT3. AKT3 has two phosphorylation sites at Threonine 305 and Serine 472. The mutation resulted in a non-synonymous amino acid substitution from aspartic acid (Asp) to valine (Val) at the amino acid position of 219 in the protein kinase domain. PH, pleckstrin homology domain. (**B**) Amino acid sequence alignment among protein kinase family. The amino acid at the Nmf350 mutation is highly conserved among protein kinase family and various species. Arrow indicates an amino acid position 219 of mouse AKT3. (**C**) No gross change of AKT3 protein levels in the brain from Nmf350 mice. Brains from two wild-type (+/+), *Nmf350* heterozygote (mt/+) and homozygote (mt/mt), were examined for the expression of AKT3 (60–70 kDa) by western blot analysis. The brain from *Akt3* knockout (KO) mouse was used for a negative control.

To investigate whether lacking *Akt3* has any effect on seizure threshold, we examined $Akt3^{tm1Mbb}$ homozygous, $Akt3^{tm1Mbb}$ heterozygous and wild-type mice. In contrast to $Akt3^{Nmf350}$, $Akt3^{tm1Mbb}$ null homozygotes showed significantly elevated seizure threshold compared with wild-type (Fig. 3; homozygous, 8.23 mA, $n = 17$; wild-type, 7.22 mA, $n = 17$; $P < 0.05$, Tukey's HSD test). Confoundingly, $Akt3^{tm1Mbb}$ heterozygotes at first appeared to have a lower seizure threshold even when compared with the wild-type. However, we recognized that the $Akt3^{tm1Mbb}$ null mutation resides in the B6J.129P2-$Akt3^{tm1Mbb}$ congenic strain that would carry 129-derived DNA flanking the *Akt3* locus, and that very closely linked to *Akt3* on Chr 1 is a major quantitative trait locus *Szs1*, from which the 129 allele would be expected to confer a lower threshold than B6J (35). To test whether the inheritance of a 129-derived background passenger allele could account for the lower seizure threshold of $Akt3^{tm1Mbb}$ heterozygotes, we determined the seizure threshold of Chr 1 congenic strain B6J.129S-$Fcgr2b^{tm1Rav}$ heterozygotes. These mice carry a null allele in the unrelated *Fcgr2b* gene—not highly expressed in the brain—and also the 129 allele of the prime candidate gene for *Szs1, Kcnj10* (35). We determined that the seizure threshold of B6J.129S-$Fcgr2b^{tm1Rav}$ heterozygotes was indeed lower than littermate controls by approximately the same amount as *Akt3* null heterozygotes (Fig. 3). From this, we conclude that similar coinheritance of *Szs1* in *Akt3* null mice is fully sufficient to explain the low seizure threshold of $Akt3^{tm1Mbb}$ heterozygotes. These results also imply that the raised seizure threshold of $Akt3^{tm1Mbb}$ homozygotes is even more striking, that is, given the linked presence of susceptible, 129-derived allele of *Szs1* which would work additively against it.

Increased brain weight and size and ectopic hippocampal neurons in $Akt3^{Nmf350}$ mice

Akt3 null mice were previously observed to have decreased brain weight and size compared with the wild-type (16,17). $Akt3^{Nmf350}$ adult heterozygous and homozygous mice were examined for body and brain weight and compared with age- and gender-matched control wild-type mice. $Akt3^{Nmf350}$ mice demonstrated significantly larger brains than the wild-type, relative to body size, across both mutant genotypes (Table 2; Fig. 4A). Conventional histology revealed no

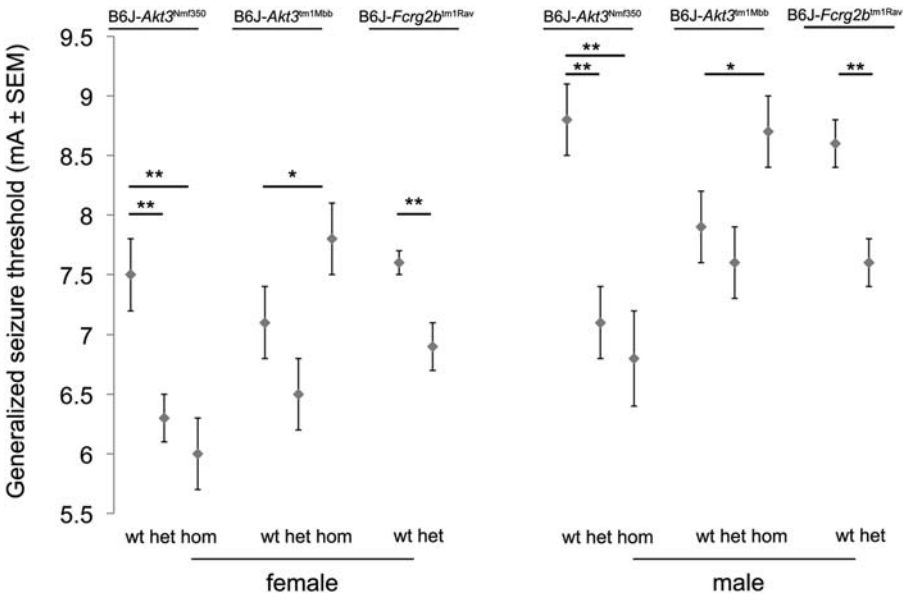

Figure 3. ECT for generalized, tonic–clonic seizures in Nmf350, *Akt3* null and congenic control mice. ECT was measured in B6J-*Akt3*^{Nmf350},B6J.129-*Akt3*^{tm1Mbb} (null) mice and B6J.129-*Fcrg2b*^{tm1Rav} congenic control adult mice (age 6–13 weeks). The mean ECT ($\pm$1SD) of *Akt3*^{Nmf350} homozygous (hom) and heterozygous (het) mice was significantly lower than that of wild-type (wt) animals, while *Akt3* null homozygotes showed higher mean ECT than wild-type littermates. The mean ECT of *Akt3* null heterozygotes was slightly lower than in the wild-type, but this same effect is also observed in the congenic control mice which also carry 129 strain-derived alleles in the interval. $^{**}P < 0.01$, $^{*}P < 0.01$ Tukey HSD test.

obvious defects in general anatomical organization but suggested of an enlarged hippocampus in the mutant brain compared with the wild-type control (Fig. 4B). Preliminary histology had also suggested the presence of ectopic neurons in the hippocampus of a homozygous mutant (data not shown). To explore this observation, immunohistochemistry for KI67, a marker of proliferating cells, and doublecortin (DCX), a marker of early differentiated neurons, were conducted on three *Akt3*^{Nmf350} homozygous, six *Akt3*^{Nmf350} heterozygous and five wild-type brains. All three homozygotes showed an excess of ectopic cellular staining in the hilus and molecular layer. Findings were most pronounced in the youngest homozygote (6 weeks) relative to older homozygotes (12 weeks), likely reflecting greater proliferation rates in younger animals (Fig. 4C). *Akt3*^{Nmf350} heterozygous mice also showed a suggestive trend towards increased numbers of ectopic cells (data not shown). Heterozygous animals were also examined for altered rates of adult hippocampal neurogenesis. A modification of the optical dissector approach was used to assess the number of KI67-positive cells from 20-week-old wild-type ($n = 4$) and *Akt3*^{Nmf350} heterozygous ($n = 5$) animals. The number of KI67-positive cells/dentate was virtually identical on each group (WT, 43.8 + 4.7; *Akt3*^{Nmf350}, 41.3 + 8.2; $P = 0.791$, Student's *t*-test), suggesting no change in proliferation rates, although changes at other time points or in homozygotes cannot be excluded. We also noticed that one of ~20 mutants studied for histology had an absent corpus callosum.

Table 1. Sensitivity of PTZ-induced seizures in B6J-*Akt3*^{Nmf350} mice[a]

	Total no. of mice[b]	No. of mice with tonic–clonic seizures	Mean latency (min)[b]	No. of mice with tonic hindlimb extension	Mean latency (min)[b]
Wild-type	7	0	–	0	–
Akt3$^{Nmf350/+}$	5	3	12.6	1	19.8
Akt3$^{Nmf350/Nmf350}$	6	5	7.0	3	8.0

[a]Each genotype group had similar number of mice from both sexes (wild-type, three females and four males; *Akt3*^{Nmf350} heterozygous, three females and two males; *Akt3*^{Nmf350} homozygous, two females and four males).
[b]Mean latency was calculated with only animals showed the corresponding response. Minutes, min.

Akt signaling in Akt3^{Nmf350} mice

The increased brain size of *Akt3*^{Nmf350} mutants, contrasted with the decrease in *Akt3* null mice, as well as the presence of ectopic hippocampal neurons prompted us to hypothesize that *Akt3*^{Nmf350} causes an increase in AKT signaling activity during development. To determine whether this associated with an increase in phosphorylation of AKT3 itself, by western blot we examined protein homogenates from whole brain, first using a pan-AKT antibody for the Ser 473 phosphorylation site. It is important to note that assessment of AKT isoform-specific function in the brain is complicated by the coexpression of the other two isoforms, AKT1 and AKT2. Nevertheless, in previous studies, a decrease in overall phospho-Akt (Ser 473) was detected in *Akt3* null mice, presumably reflecting a decreased phosphorylation level of AKT3 itself (16,17). For this reason, we thought it might be possible to observe altered phosphorylation of total AKT in *Akt3*^{Nmf350} even in the presence of AKT1 and AKT2. However, by western blot of brain

Table 2. Body and brain weight of adult (7–9 month-old) *Akt3*^{Nmf350} mice

	Female			Male		
	Body weight (g), Mean ± SD	Brain weight (g), Mean ± SD	*n*	Body weight (g), Mean ± SD	Brain weight (g), Mean ± SD	*n*
Wild-type	24.6 ± 1.25	0.460 ± 0.013	5	32.8 ± 1.69	0.442 ± 0.018	4
Akt3^{Nmf350}/+	24.6 ± 1.25	0.519 ± 0.013*	6	30.5 ± 1.60	0.545 ± 0.014**	6
Akt3$^{Nmf350/Nmf350}$	23.1 ± 1.37	0.566 ± 0.014**	5	31.3 ± 1.96	0.562 ± 0.018**	4

*$P < 0.05$, **$P < 0.01$ compared with the corresponding mean value of wild-type mice by using Tukey's HSD test.

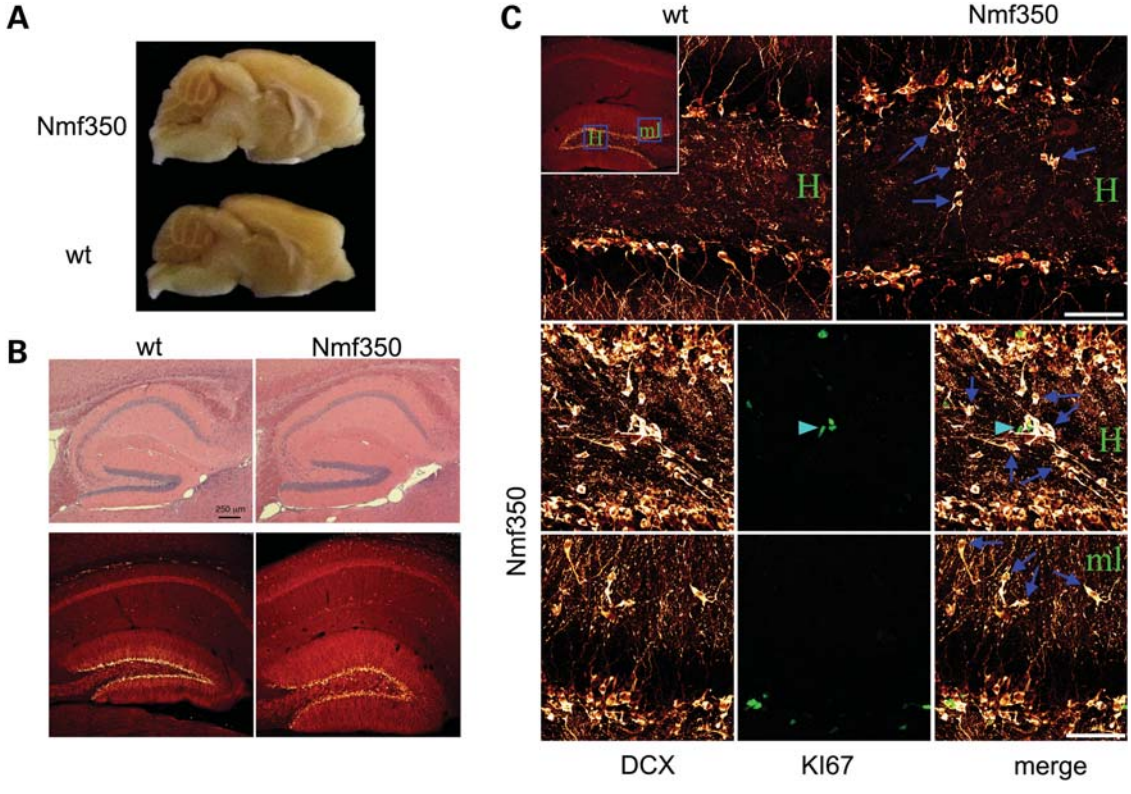

Figure 4. Increased brain size and ectopic hippocampal neurons in *Akt3*^{Nmf350} mice. (**A**) Brains were dissected from 35-week-old wild-type (WT) and *Akt3*^{Nmf350} homozygous (Nmf350) mice ($n = 3$). The mutant brain was clearly larger than that of the wild-type. (**B**) Hematoxylin and eosin (H&E) staining (top) or immunofluorescence for DCX (red) of sagittal brain sections derived from wild-type (WT) and *Akt3*^{Nmf350} homozygous (Nmf350) mice also suggested that the hippocampus was larger. (**C**) Confocal maximum projections of DCX (red) immunostaining in the hippocampus of 12-week-old wild-type and Nmf350 mice are shown in the top row. Images are from the dentate hilus (H; boxed region in inset). Hilar ectopic granule cells were rare in wild-type animals and common in Nmf350 mice (blue arrows). The middle and bottom rows show confocal projections of DCX (red) and KI67 (green) immunostaining from a younger, 6-week-old, Nmf350 mouse. In this animal, DCX immunoreactive hilar ectopic cells were more numerous relative to older animals (middle row, blue arrows) and proliferating KI67-positive cells were present in the hilus (light blue arrowhead). Ectopic granule cells (blue arrows) were also evident in the dentate molecular layer (ml, see inset for orientation). Scale bar = 50 μm.

homogenates, we found that the amount of total activated AKT was not different from the wild-type (Fig. 5). Similarly, we examined the phosphorylation level of AKT substrates, such as S6, TSC2 (tuberin) and Forkhead box O3 (FOXO3, also known as FKHRL1), but no obvious differences were observed (Fig. 5).

Therefore, because of the coexpression of three AKT isoforms in the brain, to assess the kinase activity conferred by *Akt3*^{Nmf350} we conducted an *in vitro* assay following transient expression of HA-tagged recombinant wild-type AKT3 and mutant AKT3 (NMF350 -D219V) in HEK293 cells. In five separate experiments, mutant AKT3 consistently gave an approximately 2-fold higher kinase activity than the wild-type, suggesting that the *Nmf350* mutation enhances the kinase function of AKT3 ($P < 0.05$; Fig. 6).

Although the presence of other AKT proteins is a complicating factor for detection of quantitative changes in brain homogenates, we suspected that an effect of *Akt3*^{Nmf350} would be more obvious in selected neuronal types or brain regions where the level of AKT3 is particularly high compared with the other isoforms. Immunofluorescence microscopy studies were performed on histological sections, using the antibody against phosphorylated S6. In adult brain sections, we indeed observed more cells positive for phospho-S6 in *Akt3*^{Nmf350} mice than wild-type littermates, particularly in the dentate gyrus of the hippocampus ($n = 3$ per genotype;

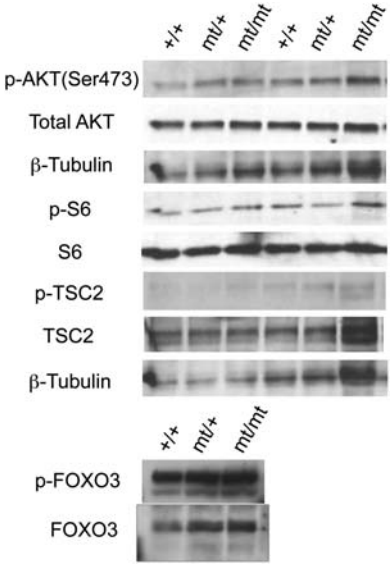

Figure 5. Western blot analysis of AKT signaling in brains from *Akt3*^{Nmf350} mice. The phosphorylation status of proteins involved in AKT signaling was investigated in cerebrum from adult wild-type mice (+/+) and *Akt3*^{Nmf350} heterozygous (mt/+) and homozygous (mt/mt) mutants ($n = 2$ in each group). No gross change was observed in *Akt3*^{Nmf350} mice. p- indicates phosphorylated protein.

Fig. 7A). Co-immunofluorescence with a mature neuronal cell marker, anti-NeuN, revealed that the majority of the phospho-S6-positive cells displayed NeuN immunoreactivity in the nucleus (Fig. 7A), indicating the subpopulation of neurons that highly expressed phospho-S6 in *Akt3*^{Nmf350} homozygotes. In other regions such as CA1 and cerebral cortex, mutants and wild-type showed similar immunoreactivity of phospho-S6 (Fig. 7B and C).

DISCUSSION

In this study, we identified a novel missense mutation, D219V, in the *Akt3* gene of Nmf350 mice. Both *Akt3*^{Nmf350} heterozygotes and homozygotes showed high susceptibility to electrical and PTZ-induced seizures, sporadic spontaneous seizures and increased brain size. We also observed KI67/DCX-positive ectopic neurons in the hippocampus in both young and adult mutants. In contrast, *Akt3* null mice showed seizure resistance, indicating that *Akt3*^{Nmf350} is unlikely to cause a loss of function. Indeed, we found that *Akt3*^{Nmf350} causes an increase of kinase activity in transfected HEK culture cells, compared with the wild-type, and we also observed an increase in immunoreactivity of phosphorylated S6 in the dentate gyrus of the hippocampus in *Akt3*^{Nmf350} homozygotes. Altogether, our results suggest that *Akt3*^{Nmf350} may increase the kinase function of AKT3, and that the isoform-specific enhanced activity of the AKT signaling pathways results in a unique phenotype in *Akt3*^{Nmf350} mice.

Akt3^{Nmf350} was mapped to an ∼1 Mb segment on mouse Chromosome 1, containing three candidate genes in addition to *Akt3*. *Cep170* was first identified as an interaction partner of Polo-like kinase 1 (*Plk1*) by using a yeast two-hybrid screen and human cells and suggested a role in the regulation of centrosome maturation during cell cycle (36). *Sdccag8* encodes NY-CO-8, which was originally found as a colon cancer autoantigen by serological analysis of recombinant cDNA expression libraries of human colon cancers and later indentified as being the C-terminal portion of human and mouse CCCAP (the centrosomal colon cancer autoantigen protein) (37). No animal studies have been reported of *Cep170* or *Sdccag8* and their functions in the brain are unknown. On the other hand, *Zfp238*, also known as *RP58*, encodes a DNA binding protein and exhibits a sequence-specific transcriptional repressor activity (38). The *RP58* transcripts are highly expressed in the cerebral cortex in the embryonic mouse brain and the expression is maintained particularly in glutamatergic neurons in adult cerebral cortex. Recently, *Zfp238* null mice have been reported to show dysplasia of the neocortex and of the hippocampus, reduction of the number of mature cortical neurons and abnormal neuronal migration within the cortical plate (39). We have sequenced all of the coding exons in these candidate genes, and no variants were found. Together with the contrasting phenotypes conferred by the dominant *Akt3*^{Nmf350} allele when compared with *Akt3* null mice, it is reasonable to conclude that the D219V mutation in *Akt3* is the cause of the phenotypes in *Nmf350* mutants.

AKT3 is the predominant AKT isoform in the adult mammalian brain, accounting for ∼50% of the total AKT in the cerebral cortex and hippocampus (16). Mouse knockouts of *Akt3* have been reported from two separate groups (16,17). Both studies demonstrated that the disruption of *Akt3* leads to selective reduction of brain weight in adult mice, which presumably results from smaller and fewer cells than those in the normal brain. Because the brain weight of newborn mice showed no difference between *Akt3* null and wild-type animals, it has been suggested that *Akt3* has an essential role in postnatal brain development. No other anatomical malformations of the brain were observed except for a thinning of the corpus callosum reported by the one group (17). In contrast to *Akt3* null mice, the brain weight of *Akt3*^{Nmf350} mice was significantly increased, and there was suggestive enlargement of the hippocampus and particularly in *Akt3*^{Nmf350} homozygotes, notable DCX-positive and K167-positive ectopic neurons in the hilus and the molecular layer. However, the question of whether the increase in brain weight results from an increase in cell size and/or cell number remains to be investigated. The PI3K and TOR kinases play a central role in the signaling network controlling growth of organisms, and PTEN negatively regulates this pathway (40). Selective deletion of *Pten* in specific neuronal populations causes progressive macrocephaly with seizures and ataxia in mice (12,13). In the mutants, neurons lacking *Pten* expressed high levels of phosphorylated AKT and S6, and showed an increase of soma size. In addition, rapamycin treatment strongly suppressed both seizure activities and hypertrophy of cortical neurons in *Pten* mutants. Although the specific isoform of AKT and other AKT-independent pathways were not addressed in those studies, the loss of *Pten* could globally affect its downstream pathways that are present in the selected neurons, resulting in marked phenotypes such as frequent spontaneous seizures and neuronal hypertrophy (approximately 2-fold increase in brain mass in adult mice).

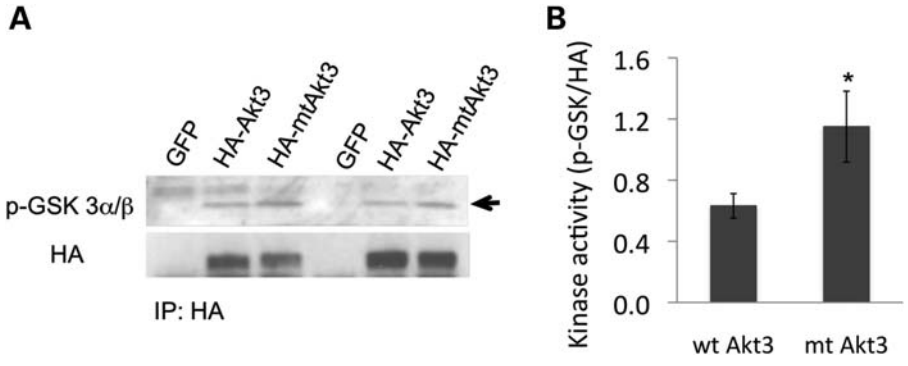

Figure 6. Immunoprecipitation kinase assay with recombinant AKT3 and mutant AKT3 (D219V). HA-tagged wild-type AKT3 or mutant AKT3 (D219V) protein was transiently expressed in HEK293 cells and purified with the HA antibody for the kinase assay. The recombinant GSK3 protein was used as a substrate. (**A**) Representative results from five separate *in vitro* kinase assays. The amount of both phosphorylated substrates and existent HA-tagged AKT3 proteins were measured by western blot analysis. Arrow indicates the specific band of p-GSK3α/β at 27 kDa. (**B**) The mean kinase activity of wt AKT3 and mt AKT3. Kinase activity was assessed as a relative band intensity of p-GSK to HA and compared between wt and mt AKT3 by a paired *t*-test (wt Akt3, 0.63 ± 0.18; mt Akt3, 1.15 ± 0.52, $n = 5$ in each group, $P = 0.0410$).

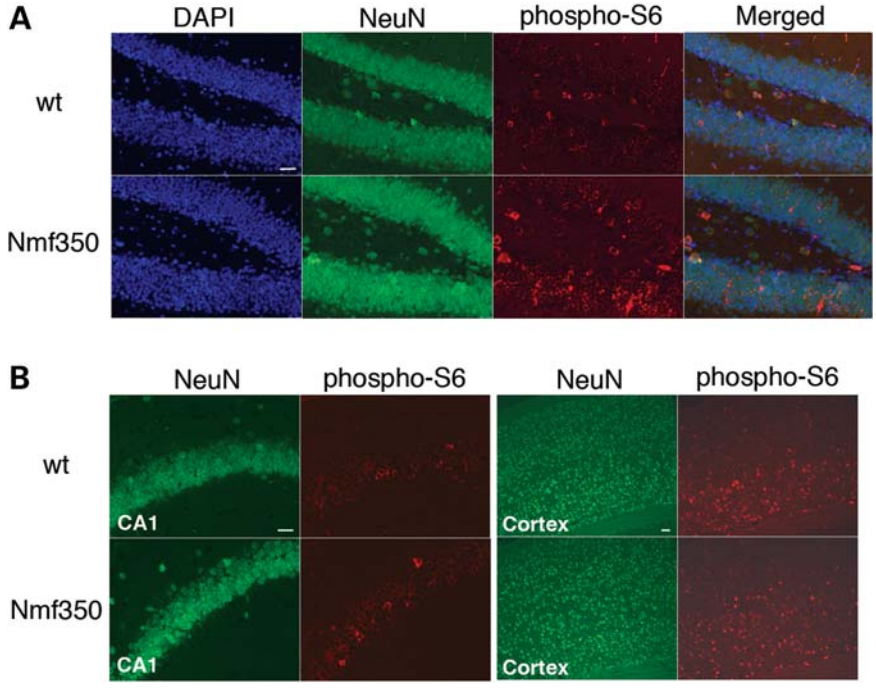

Figure 7. Increased expression of phosphorylated S6 protein in the $Akt3^{Nmf350}$ hippocampus. Sections of adult wild-type (wt) and $Akt3^{Nmf350}$ homozygous (Nmf350) mice were immunostained with the antibodies against phospho-S6 and NeuN. Elevated levels of phosphorylated S6 were seen in the dentate gyrus of Nmf350 mice when compared with wild-type animals (**A**). Those cells were also NeuN positive. Phospho-S6-positive neurons were occasionally or broadly seen in the CA1 (**B**) or cerebral cortex (**C**) area in both $Akt3^{Nmf350}$ and wild-type animals with the same level, respectively. Scale bars indicate 50 μm.

Compared with the *Pten* mutants, we observed a relatively mild phenotype in $Akt3^{Nmf350}$ mice: an ∼1.2-fold increase in brain size without obvious abnormal cell morphology, and sporadic spontaneous seizures. The relative subtlety may be due to the possibility that the $Akt3^{Nmf350}$ mutation affects signaling events dependent solely on AKT3 activity. Moreover, total AKT phosphorylation was not altered in the $Akt3^{Nmf350}$ cerebrum, while in the previous study the inactivation of *Akt3* did lower the amount of phosphorylated AKT in the brain with a 38% reduction (17). In addition, our immunofluorescence study showed moderate but not excessive increase in phospho-S6 signal in the $Akt3^{Nmf350}$ hippocampus. Together, these results suggest that $Akt3^{Nmf350}$ is unlikely to be constitutively active but rather has increased kinase activity, potentially in an activity-dependent manner. Indeed, we have examined phospho-S6 in animals treated with PTZ. Preliminary results suggest that a low dose of PTZ (20 mg/kg) caused an increased activation of phospho-S6 in the brain of $Akt3^{Nmf350}$ mice compared with wild-type littermates (data not shown). Further research is required to understand how $Akt3^{Nmf350}$ increases the AKT3 kinase function.

The present study provides the novel observation that *Akt3* can affect seizure susceptibility—showing higher seizure threshold in the *Akt3* null, or lower seizure threshold and sporadic convulsions in Nmf350 mutant. This generally supports the idea that AKT signaling is implicated in epilepsy. The underlying mechanism and specific target substrates, however, remain unknown. It is an important question whether seizure susceptibility in *Akt3*^{Nmf350} mutants is directly related to abnormal synaptic transmission or neuronal cell survival mediated by PI3K/AKT/mTOR pathways, or is a secondary result of abnormal brain development, involving cell proliferation, migration and/or synaptogenesis. Indeed, the presence of DCX- and KI67-positive ectopic hippocampal neurons suggests a developmental abnormality perhaps affecting neuronal migration or localization; the low penetrance absent corpus callosum phenotype is also consistent with an early defect. Studies using young animals and/or conditional gene targeting will be critical to ascertain causally the developmental effect of AKT3 levels on seizures.

In summary, the *Akt3*^{Nmf350} allele confers an increase in AKT3 activity in specific neuronal populations in the brain, resulting in a unique dominant phenotype distinct from *Akt3* null mice and all other known mouse models related to PI3K/AKT pathways. Nmf350 mice provide a new and unique tool for studying physiological roles of AKT signaling in the brain, and potentially novel mechanisms for seizure susceptibility.

MATERIALS AND METHODS

Animals

Nmf350 mice were generated by ENU mutagenesis in The Jackson Laboratory NMF on the C57BL/6J (B6J) background as described previously (8). Briefly, B6J males were injected intraperitoneally at 8–10 weeks of age with either 2 × 100, 2 × 110, 2 × 120, 3 × 80 or 3 × 85 mg/kg ENU. Following a 10-week sterility period, each ENU-treated B6J male (G_0) was mated with B6J females to generate G_1 males. The G_1 males were used in a three-generation breeding scheme, where G_1 males were mated with B6J females to generate G_2 daughters that were backcrossed to their G_1 fathers in order to produce G_3 offspring recessive for ENU-induced mutations. The ECT test was performed on G_3 mice, as described in more detail below.

B6J and BALB/cByJ inbred mice were obtained from The Jackson Laboratory. *Akt3* knockout mice were bred at the University of Pennsylvania with heterozygous and wild-type littermates. To generate congenic *Akt3*^{Nmf350} mice on the BALB background, B6J-*Akt3*^{Nmf350} heterozygotes were outcrossed to BALB mice and heterozygous F_1 hybrids were repeatedly backcrossed to BALB mice by using flanking simple sequence length polymorphisms (SSLPs) that distinguished BALB from B6J. Congenic strain B6J.129S-*Fcgr2b*^{tm1Rav} was provided by Dr Derry Roopenian. By genotyping for 129 versus B6J alleles at the microsatellite markers *D1Mit105* and *D1Mit166*, which flank both *Fcgr2b* and *Kcnj10*, the candidate gene for *Szs1*, we can infer that this congenic strain carries the 129 (susceptible) alleles of *Szs1*. F_1 hybrids of congenic B6J.129S-*Fcgr2b*^{tm1Rav} and B6J animals were backcrossed to B6J mice to obtain heterozygotes and wild-type littermates. All mice used in this study were housed at The Jackson Laboratory or The University of Pennsylvania. All animal procedures were approved by respective Institutional Animal Care and Use Committees (IACUC).

Genetic and mutational analysis

The *Akt3*^{Nmf350} mutation was originally mapped in a backcross population: (B6J-*Nmf350* x BALB)F_1 X BALB. Backcross mice were assessed for generalized, tonic–clonic seizures (previously described as 'minimal forebrain clonic seizures') using a modified Racine scale (the key endpoints were seizure grade: 0, no observable symptoms; 3, generalized, tonic–clonic seizures consisting of rearing, forelimb and jaw clonus, loss of posture, neck flexion and Straub tail; 5, tonic extension of the hindlimbs). For the whole genome scan, 44 backcross mice were genotyped for 93 SNP markers across the genome (KBiosciences, Cambridge, UK) and the data were analyzed in Mapmanager QTX for associations between marker genotype and combined seizure score. For confirmation, additional backcross mice were added—making a total of 58—and all backcross DNAs were genotyped further with SSLP markers on Chromosome 1. Several hundred additional recombinant progeny were genotyped with 22 SSLPs for fine mapping, including *D1Frk9* (forward primer, 5′-GAATAAACCTGACCCAGTTGT and reverse primer, 5′-AGTGTCTGGTGGCTGAAACA); specific N_2 animals with recombinations within the critical interval were progeny tested by crossing to BALB, and N_3 progeny were ECT tested to determine the minimal critical interval.

Genotyping of Akt3^{Nmf350} and Akt3 knockout mice

Genotyping for *Akt3*^{Nmf350} was performed by PCR or PCR followed by sequencing. For the PCR assay, the wild-type allele was amplified with forward primer, 5′-GAAATATTCCTTCCAGACAAAAGAC, and reverse primer (Akt3 × 8R), 5′-AGACCTGCTGTGGAGCTGAG, and the mutant allele was amplified with forward primer, 5′-GAAATATTCCTTCCAGACAAAAGTC and reverse primer, Akt3 × 8R. The products were distinguished on a 2% agarose gel. For sequencing-based genotyping, a 260 bp region in exon 8 containing the Nmf350 mutation was amplified with forward primer 5′-AGTGCTCATCACA ACTACCAAA and reverse primer 5′-GCCATCTTTG TCTACTCAACAGG. Subsequently, PCR products were sequenced by The Jackson Laboratory core DNA sequence service on an ABI 3730xl DNA analyzer. *Akt3* null mice were genotyped as previously described (Easton 2005).

ECT test

ECT was determined as previously described (31). Briefly, animals at 6 weeks of age or given age in the text were stimulated via silver transcorneal electrodes using an electroconvulsive stimulator (Ugo Basile Model 7801) modified as described previously and using a topical anesthetic (31). For phenotype detection, strain development and genetic mapping, each animal was tested once per day at a single

sub-threshold level corresponding to the 3% response level for wild-type B6J mice and evaluated using categorical seizure endpoints. After the strain was developed, the seizure threshold of individual animals was determined by sequential daily testing until the threshold was reached, and the mean threshold was calculated for each genotype group.

PTZ-induced seizure test

Mice were subcutaneously injected with a dose of PTZ (40 mg/kg), and monitored for 30 min. Latencies to the first three occurrences of the following seizure endpoints were recorded: twitch or myoclonic jerk, abortive tonic clonic seizure (i.e. twitch followed by ventral flexion of the neck and Straub tail, without further progression), generalized tonic clonic seizure and tonic hindlimb extension.

Western blot analysis

Protein extracts in lysis buffer [20 mM Tris (pH 7.2), 150 mM NaCl, 1 mM EDTA, 1% NP40, 10 mM NaF, 1 mM Na3VO4, 10% glycerol, complete protease inhibitor cocktail (Roche, Mannheim, Germany) and Halt^{TM} phosphatase inhibitor single-use cocktail (Thermo Scientific)] were obtained from cerebrum homogenates, resolved by SDS gradient PAGE and transferred to nitrocellulose membranes. Blots were probed with the primary antibodies and reacted with the secondary antibodies. Protein bands were detected using the ECL-plus chemiluminescent reagent (Amersham Biosciences). The antibodies against phospho-AKT (Ser 473), AKT, AKT3, phospho-S6 (Ser 235/236), S6, phospho-FOXO3, FOXO3 and phospho-TSC2 were purchased from Cell Signaling Technology. The antibodies against TSC2 were purchased from Santa Cruz.

Plasmid construction of HA-mutant (mt) Akt3 (D219V) and transfection of culture cells

The *Akt3^{Nmf350}* mutation (D219V) was introduced in pcDNA3.1-HA-murine Akt3 by a PCR-based site-directed mutagenesis method (41), using mutagenic primers 5′-CCTTCCAGACAAAAGTCCGTTTGTG and 5′-CAC AAACGGACTTTTGTCTGGAAGG, and flanking primers 5′-TAATACGACTCATATAGGG and 5′-TAGAAGG CACAGTCGAGG. The mutation was confirmed by sequencing. HEK293 cells were maintained in DMEM medium with 10% fetal bovine serum at 37°C with 5% CO_2. Cells were transfected with GFP, HA-Akt3 or HA-mt-Akt3 plasmid using lipofectamine 2000 (Invitrogen) according to the manufacturer's instructions. Forty-eight hours after transfection, cells were serum deprived for 10 h and treated with insulin (500 nM; 15 min). Treated cells were harvested in a lysis buffer. The protein lysates was used for the following kinase assay.

Kinase assay

The AKT Kinase Assay Kit (Cell Signaling Technology) was used according to the manufacturer's instructions with slight modifications. Briefly, cell lysates were immunoprecipitated with the HA agarose-conjugated antibody (Sigma). The immunoprecipitates were incubated for 30 min at 30°C in 40 μl of kinase buffer supplemented with 200 μM ATP and 1 μg of GSK3 fusion protein (CGPKGPGRRGRRRTSSFAEG), as substrate. Samples were analyzed by SDS–PAGE and blotted on nitrocellulose membranes. The level of phosphorylated GSK3 was detected with the phospho-GSK3 alpha/beta (Ser 21/9) antibody. After stripping, blots were re-probed with the HA antibody and analyzed for normalizations. Experiments were repeated five times and the relative band intensity of phospho-GSK3 versus HA was compared between wild-type AKT and mutant AKT by matched pairs Student's *t*-test using JMP software (SAS Institute Inc., Cary, NC, USA).

Histology and immunofluorescence

Mice were perfused transcardially with 4% paraformaldehyde (PFA) in PBS. Following post-fix in 4% PFA overnight, brains were embedded in paraffin and cut into 6-μm sections, or were cryoprotected in 20% sucrose (v/w) overnight and then cut into 20-μm sections on a cryostat. Paraffin sections were stained with hematoxylin and eosin (H&E). Immunofluorescence studies were carried out using both paraffin and cryo sections. The primary antibodies were diluted in PBS with 0.3% Triton X-100: phospho-S6 (1:100, Cell Signaling) and NeuN (1:100, Millipore). Microwave antigen retrieval was performed for paraffin sections prior to blocking. After overnight incubation at 4°C, the primary antibodies were detected with secondary antibodies conjugated with Alex Fluor 488 or 555 (1:1000, Invitrogen). Slides were counterstained with DAPI. DCX and KI67 immunostaining were conducted on perfusion-fixed brains (as above) sectioned at 40 μm on a cryostat and mounted to gelatin-coated slides. Slides were blocked in PBS with 0.5% Igepal and 5% donkey serum, followed by an overnight incubation in DCX (1:400, SC-8066, Santa Cruz Biotechnology) and KI67 (1:100, VP-RM04, Vector Labs) primary antibodies at 4°C. Slides were rinsed in blocker and incubated for 4 h in Alex Fluor 488 and 555 secondary antibodies (1:750). Slides were then dehydrated in alcohols, cleared in xylenes and mounted with Krystalon (Fisher Scientific). Images of doublecortin and KI67 immunoreactivity were captured with an SP5 confocal microscope set up on a DMI6000 stand (Leica Microsystems) equipped with ×10 (NA, 0.3) and ×63 (NA, 1.4) objectives.

ACKNOWLEDGEMENTS

We thank Carolyne Dunbar, Michael McCluskey, Zak Strassberg and Louise Dionne for technical assistance, and Lucy Rowe and Mary Barter of The Jackson Laboratory Fine Mapping Group for assistance with the genome scan. We are also grateful to Dr Derry Roopenian and Mr Thomas Sproule for providing B6J.129S-*Fcgr2b^{tm1Rav}* mice, and to Drs Greg Cox and Patsy Nishina for critical review of this manuscript.

Conflict of Interest statement. None declared.

FUNDING

This work was subsidized by a cancer core center grant from the National Cancer Institute (grant CA034196). The initial part of this work was funded as part of The Jackson Laboratory Neuroscience Mutagenesis Facility (NMF), cooperative agreement U01 NS41215. S.T. was supported in part by an Epilepsy Foundation of America Fellowship and in part by a Jackson Laboratory Postdoctoral Fellowship. W.N.F. was funded by grants from the National Institutes of Health (grant numbers NS031348, NS041215). M.J.B. was funded by a grant from the National Institutes of Health (grant number DK56886). S.C.D. was funded by a grant from the National Institutes of Health (grant number NS-065020).

REFERENCES

1. Gardiner, R.M. (2000) Impact of our understanding of the genetic aetiology of epilepsy. *J. Neurol.*, **247**, 327–334.
2. Lucarini, N., Verrotti, A., Napolioni, V., Bosco, G. and Curatolo, P. (2007) Genetic polymorphisms and idiopathic generalized epilepsies. *Pediatr. Neurol.*, **37**, 157–164.
3. Buchner, D.A., Seburn, K.L., Frankel, W.N. and Meisler, M.H. (2004) Three ENU-induced neurological mutations in the pore loop of sodium channel Scn8a (Na(v)1.6) and a genetically linked retinal mutation, rd13. *Mamm. Genome*, **15**, 344–351.
4. Jablonski, M.M., Dalke, C., Wang, X., Lu, L., Manly, K.F., Pretsch, W., Favor, J., Pardue, M.T., Rinchik, E.M., Williams, R.W. *et al.* (2005) An ENU-induced mutation in Rs1h causes disruption of retinal structure and function. *Mol. Vis.*, **11**, 569–581.
5. Keays, D.A., Tian, G., Poirier, K., Huang, G.J., Siebold, C., Cleak, J., Oliver, P.L., Fray, M., Harvey, R.J., Molnar, Z. *et al.* (2007) Mutations in alpha-tubulin cause abnormal neuronal migration in mice and lissencephaly in humans. *Cell*, **128**, 45–57.
6. Kermany, M.H., Parker, L.L., Guo, Y.K., Miller, D., Swanson, D.J., Yoo, T.J., Goldowitz, D. and Zuo, J. (2006) Identification of 17 hearing impaired mouse strains in the TMGC ENU-mutagenesis screen. *Hear. Res.*, **220**, 76–86.
7. Nolan, P.M., Peters, J., Strivens, M., Rogers, D., Hagan, J., Spurr, N., Gray, I.C., Vizor, L., Brooker, D., Whitehill, E. *et al.* (2000) A systematic, genome-wide, phenotype-driven mutagenesis programme for gene function studies in the mouse. *Nat. Genet.*, **25**, 440–443.
8. Yang, Y., Beyer, B.J., Otto, J.F., O'Brien, T.P., Letts, V.A., White, H.S. and Frankel, W.N. (2003) Spontaneous deletion of epilepsy gene orthologs in a mutant mouse with a low electroconvulsive threshold. *Hum. Mol. Genet.*, **12**, 975–984.
9. Meikle, L., Talos, D.M., Onda, H., Pollizzi, K., Rotenberg, A., Sahin, M., Jensen, F.E. and Kwiatkowski, D.J. (2007) A mouse model of tuberous sclerosis: neuronal loss of Tsc1 causes dysplastic and ectopic neurons, reduced myelination, seizure activity, and limited survival. *J. Neurosci.*, **27**, 5546–5558.
10. Zeng, L.H., Rensing, N.R. and Wong, M. (2009) The mammalian target of rapamycin signaling pathway mediates epileptogenesis in a model of temporal lobe epilepsy. *J. Neurosci.*, **29**, 6964–6972.
11. Zeng, L.H., Rensing, N.R. and Wong, M. (2009) Developing antiepileptogenic drugs for acquired epilepsy: targeting the mammalian target of rapamycin (mTOR) pathway. *Mol. Cell Pharmacol.*, **1**, 124–129.
12. Backman, S.A., Stambolic, V., Suzuki, A., Haight, J., Elia, A., Pretorius, J., Tsao, M.S., Shannon, P., Bolon, B., Ivy, G.O. *et al.* (2001) Deletion of Pten in mouse brain causes seizures, ataxia and defects in soma size resembling Lhermitte-Duclos disease. *Nat. Genet.*, **29**, 396–403.
13. Kwon, C.H., Zhu, X., Zhang, J., Knoop, L.L., Tharp, R., Smeyne, R.J., Eberhart, C.G., Burger, P.C. and Baker, S.J. (2001) Pten regulates neuronal soma size: a mouse model of Lhermitte-Duclos disease. *Nat. Genet.*, **29**, 404–411.
14. Brazil, D.P., Yang, Z.Z. and Hemmings, B.A. (2004) Advances in protein kinase B signalling: AKTion on multiple fronts. *Trends Biochem. Sci.*, **29**, 233–242.
15. Franke, T.F. (2008) PI3K/Akt: getting it right matters. *Oncogene*, **27**, 6473–6488.
16. Easton, R.M., Cho, H., Roovers, K., Shineman, D.W., Mizrahi, M., Forman, M.S., Lee, V.M., Szabolcs, M., de Jong, R., Oltersdorf, T. *et al.* (2005) Role for Akt3/protein kinase Bgamma in attainment of normal brain size. *Mol. Cell Biol.*, **25**, 1869–1878.
17. Tschopp, O., Yang, Z.Z., Brodbeck, D., Dummler, B.A., Hemmings-Mieszczak, M., Watanabe, T., Michaelis, T., Frahm, J. and Hemmings, B.A. (2005) Essential role of protein kinase B gamma (PKB gamma/Akt3) in postnatal brain development but not in glucose homeostasis. *Development*, **132**, 2943–2954.
18. Wang, Q., Liu, L., Pei, L., Ju, W., Ahmadian, G., Lu, J., Wang, Y., Liu, F. and Wang, Y.T. (2003) Control of synaptic strength, a novel function of Akt. *Neuron*, **38**, 915–928.
19. Chen, H.K., Fernandez-Funez, P., Acevedo, S.F., Lam, Y.C., Kaytor, M.D., Fernandez, M.H., Aitken, A., Skoulakis, E.M., Orr, H.T., Botas, J. *et al.* (2003) Interaction of Akt-phosphorylated ataxin-1 with 14-3-3 mediates neurodegeneration in spinocerebellar ataxia type 1. *Cell*, **113**, 457–468.
20. Humbert, S., Bryson, E.A., Cordelieres, F.P., Connors, N.C., Datta, S.R., Finkbeiner, S., Greenberg, M.E. and Saudou, F. (2002) The IGF-1/Akt pathway is neuroprotective in Huntington's disease and involves Huntingtin phosphorylation by Akt. *Dev. Cell*, **2**, 831–837.
21. Wu, H., Lu, D., Jiang, H., Xiong, Y., Qu, C., Li, B., Mahmood, A., Zhou, D. and Chopp, M. (2008) Increase in phosphorylation of Akt and its downstream signaling targets and suppression of apoptosis by simvastatin after traumatic brain injury. *J. Neurosurg.*, **109**, 691–698.
22. Wu, H., Lu, D., Jiang, H., Xiong, Y., Qu, C., Li, B., Mahmood, A., Zhou, D. and Chopp, M. (2008) Simvastatin-mediated upregulation of VEGF and BDNF, activation of the PI3K/Akt pathway, and increase of neurogenesis are associated with therapeutic improvement after traumatic brain injury. *J. Neurotrauma*, **25**, 130–139.
23. Piermartiri, T.C., Vandresen-Filho, S., de Araujo Herculano, B., Martins, W.C., Dal'agnolo, D., Stroeh, E., Carqueja, C.L., Boeck, C.R. and Tasca, C.I. (2009) Atorvastatin prevents hippocampal cell death due to quinolinic acid-induced seizures in mice by increasing Akt phosphorylation and glutamate uptake. *Neurotox. Res.*, **16**, 106–115.
24. Zhang, X., Chen, Y., Ikonomovic, M.D., Nathaniel, P.D., Kochanek, P.M., Marion, D.W., DeKosky, S.T., Jenkins, L.W. and Clark, R.S. (2006) Increased phosphorylation of protein kinase B and related substrates after traumatic brain injury in humans and rats. *J. Cereb. Blood Flow Metab.*, **26**, 915–926.
25. Cho, H., Mu, J., Kim, J.K., Thorvaldsen, J.L., Chu, Q., Crenshaw, E.B. 3rd, Kaestner, K.H., Bartolomei, M.S., Shulman, G.I. and Birnbaum, M.J. (2001) Insulin resistance and a diabetes mellitus-like syndrome in mice lacking the protein kinase Akt2 (PKB beta). *Science*, **292**, 1728–1731.
26. Cho, H., Thorvaldsen, J.L., Chu, Q., Feng, F. and Birnbaum, M.J. (2001) Akt1/PKBalpha is required for normal growth but dispensable for maintenance of glucose homeostasis in mice. *J. Biol. Chem.*, **276**, 38349–38352.
27. Yang, Z.Z., Tschopp, O., Hemmings-Mieszczak, M., Feng, J., Brodbeck, D., Perentes, E. and Hemmings, B.A. (2003) Protein kinase B alpha/Akt1 regulates placental development and fetal growth. *J. Biol. Chem.*, **278**, 32124–32131.
28. Davies, M.A., Stemke-Hale, K., Tellez, C., Calderone, T.L., Deng, W., Prieto, V.G., Lazar, A.J., Gershenwald, J.E. and Mills, G.B. (2008) A novel AKT3 mutation in melanoma tumours and cell lines. *Br. J. Cancer*, **99**, 1265–1268.
29. Kwon, C.H., Zhu, X., Zhang, J. and Baker, S.J. (2003) mTor is required for hypertrophy of Pten-deficient neuronal soma *in vivo*. *Proc. Natl Acad. Sci. USA*, **100**, 12923–12928.
30. Ljungberg, M.C., Sunnen, C.N., Lugo, J.N., Anderson, A.E. and D'Arcangelo, G. (2009) Rapamycin suppresses seizures and neuronal hypertrophy in a mouse model of cortical dysplasia. *Dis. Model Mech.*, **2**, 389–398.
31. Frankel, W.N., Taylor, L., Beyer, B., Tempel, B.L. and White, H.S. (2001) Electroconvulsive thresholds of inbred mouse strains. *Genomics*, **74**, 306–312.
32. Boumil, R.M., Letts, V.A., Roberts, M.C., Lenz, C., Mahaffey, C.L., Zhang, Z.W., Moser, T. and Frankel, W.N. (2010) A missense mutation in a highly conserved alternate exon of dynamin-1 causes epilepsy in fitful mice. *PLoS Genet.*, **6**, e1001046.

33. Frankel, W.N., Taylor, B.A., Noebels, J.L. and Lutz, C.M. (1994) Genetic epilepsy model derived from common inbred mouse strains. *Genetics*, **138**, 481–489.
34. Rise, M.L., Frankel, W.N., Coffin, J.M. and Seyfried, T.N. (1991) Genes for epilepsy mapped in the mouse. *Science*, **253**, 669–673.
35. Ferraro, T.N., Golden, G.T., Smith, G.G., Martin, J.F., Lohoff, F.W., Gieringer, T.A., Zamboni, D., Schwebel, C.L., Press, D.M., Kratzer, S.O. *et al.* (2004) Fine mapping of a seizure susceptibility locus on mouse Chromosome 1: nomination of Kcnj10 as a causative gene. *Mamm. Genome*, **15**, 239–251.
36. Guarguaglini, G., Duncan, P.I., Stierhof, Y.D., Holmstrom, T., Duensing, S. and Nigg, E.A. (2005) The forkhead-associated domain protein Cep170 interacts with Polo-like kinase 1 and serves as a marker for mature centrioles. *Mol. Biol. Cell*, **16**, 1095–1107.
37. Kenedy, A.A., Cohen, K.J., Loveys, D.A., Kato, G.J. and Dang, C.V. (2003) Identification and characterization of the novel centrosome-associated protein CCCAP. *Gene*, **303**, 35–46.
38. Aoki, K., Meng, G., Suzuki, K., Takashi, T., Kameoka, Y., Nakahara, K., Ishida, R. and Kasai, M. (1998) RP58 associates with condensed chromatin and mediates a sequence-specific transcriptional repression. *J. Biol. Chem.*, **273**, 26698–26704.
39. Okado, H., Ohtaka-Maruyama, C., Sugitani, Y., Fukuda, Y., Ishida, R., Hirai, S., Miwa, A., Takahashi, A., Aoki, K., Mochida, K. *et al.* (2009) The transcriptional repressor RP58 is crucial for cell-division patterning and neuronal survival in the developing cortex. *Dev. Biol.*, **331**, 140–151.
40. Neufeld, T.P. (2003) Body building: regulation of shape and size by PI3K/TOR signaling during development. *Mech. Dev.*, **120**, 1283–1296.
41. Heckman, K.L. and Pease, L.R. (2007) Gene splicing and mutagenesis by PCR-driven overlap extension. *Nat. Protoc.*, **2**, 924–932.